Primljen / Received: 13.7.2019.
Ispravljen / Corrected: 15.1.2020.
Prihvaćen / Accepted: 8.5.2020.
Dostupno online / Available online: 10.5.2021.

Experimental investigation of exterior reinforced concrete beam - column joints strengthened with hybrid FRP laminates

Authors:

Sumathi Marimuthu, MSc. CE
Anna University, Tamilnadu, India
Faculty of Civil Engineering
sumathimarimuthu20@gmail.com
Corresponding author

Assoc.Prof. **Greeshma Sivasankara Pillai**, PhD. CE
Anna University, Tamilnadu, India
Faculty of Civil Engineering
greeshmasspillai@yahoo.co.in

Research Paper

Sumathi Marimuthu, Greeshma Sivasankara Pillai

Experimental investigation of exterior reinforced concrete beam - column joints strengthened with hybrid FRP laminates

In the present study, an experimental and theoretical investigation is carried out on the reinforced concrete exterior beam-column joints strengthened with the hybrid fibre reinforced polymer (HFRP). The effect of reversible distress that develops in the joint region due to seismic force is determined experimentally by applying reverse cyclic loading on the tip of the beam. In theoretical analysis, the shear strength of strengthened joints was determined, and satisfactory correlations with experimental results were established. Hence, the proposed physical model provides valuable insight into the strength behaviour of the joints.

Key words:
exterior beam-column joint, hybrid fibre reinforced polymer (HFRP) lamination, glass fibre reinforced polymer

Prethodno priopćenje

Sumathi Marimuthu, Greeshma Sivasankara Pillai

Eksperimentalno istraživanje vanjskih armiranobetonskih spojeva greda-stup ojačanih hibridnim FRP lamelama

U ovom je radu prikazano eksperimentalno i teoretsko istraživanje armiranobetonskih vanjskih spojeva greda-stup pojačanih hibridnim vlaknima-armiranim polimerom (HFRP). Utjecaj povratnog oštećenja do kojeg dolazi u području spoja zbog seizmičkih sila definiran je eksperimentalno nanošenjem reverzibilnog cikličnog opterećenja na vrh grede. U okviru teoretske analize određena je posmična čvrstoća pojačanih spojeva te je utvrđena zadovoljavajuća podudarnost s eksperimentalnim rezultatima. Stoga predloženi fizikalni model pruža vrijedne spoznaje o čvrstoći spojeva.

Ključne riječi:
vanjski spoj greda-stup, hibridni polimer ojačan vlaknima (HFRP) laminat, polimer ojačan staklenim vlaknima

Vorherige Mitteilung

Sumathi Marimuthu, Greeshma Sivasankara Pillai

Experimentale Forschung von Außen-Stahlbetonbalkenverbindungen – Säule, welche mit den hybriden FRP-Lamellen verstärkt wurden

In dieser Arbeit wurde die experimentale und theoretische Forschung von Außen-Stahlbetonbalkenverbindungen – Säulen, welche mit den Hybridfasern – mit dem armierten Polymer (HFRP) verstärkt wurden – dargestellt. Der Einfluss der Rückbeschädigung, zu welcher es auf dem Gebiet der Verbindung wegen der seismischen Kräfte kommt, wurde experimental definiert, und zwar durch die Übertragung der reversiblen zyklischen Belastung auf die Spitze des Balkens. Im Rahmen der theoretischen Analyse wurde die Schiebefestigkeit der verstärkten Verbindungen festgelegt, und es wurde die zufriedenstellende Übereinstimmung mit den experimentalen Ergebnissen festgestellt. Aus diesem Grund bietet das vorgeschlagene physikalische Modell die wertvollen Erkenntnisse über die Festigkeit von Verbindungen.

Schlüsselwörter:
Außenbalkenverbindung-Säule, Hybrid-Polymer, welches mit den Fasern (HFRP) verstärkt wurde – Laminat, Polymer, welches mit den Glasfasern verstärkt wurde

1. Introduction

Most old structures have been designed and constructed for gravity loads. In reinforced concrete framed structures, the most critical component is the exterior beam-column joint which is susceptible to severe environmental conditions. Many researchers have made an extensive study of past earthquakes, with the focus on the causes and reasons for failure in the beam-column joint.

Kaushik and Jain [1], Saatcioglu et al. [2] observed that during the Sumatra earthquake (2004) the damage caused to the reinforced concrete structure was due to a lack of proper seismic design and detailing. In Bhuj Earthquake (2001) there was severe damage to the exterior beam-column joints due to the instability of the column. The instability was caused due to disorganization and insufficient longitudinal and shear reinforcements. Two major modes of failure at the joints are (a) joint shear failure, and (b) end anchorage failure (Ghobarah and Said, [3]). From the survey of past earthquakes, it can be observed that beam-column joints in reinforced framed structures are crucial zones for an effective transfer of load between structural connections (i.e. beams and columns). For the gravity load design practice, the design check for joints is not necessary as they are not critical. The failure of reinforced framed structures is due to heavy distress caused by the joint shear resulting in failure of the building.

One of techniques that are used to rehabilitate structures damaged in earthquakes is by means of repair and retrofitting. Past research shows that Fibre Reinforced Polymers (FRP) can be used for retrofitting the exterior, interior, and corner beam-column joints due to the ease of application, cost-effectiveness and high corrosion resistance, low unit weight, high tensile strength to stiffness ratio and excellent fatigue behaviour (Ozcan et al. [4]). Antonopoulos and Triantafillou [5] pointed out that the presence of the transverse beam strongly affects the FRP influence on beam-column joints. Attari et al. [6] studied the effect of the external strengthening of beam-column joints using different types of fibre reinforced composites. The shear strength and ductility could be improved with the combination of carbon and glass fibre reinforced polymers. The external bonding of FRP sheets with epoxy resin is an easy retrofitting technique for the reinforced concrete beam-column joint subjected to seismic loads (Engindeniz et al. [7]). Mosallam and Banerjee [8], Parvin and Granata [9], Said and Nehdi [10], Mukherjee and Joshi [11], and Parvin and Wu [12] have noted that strengthening of connections can increase the moment capacity, ductility, initial stiffness, energy dissipation capacity, and reduce joint rotations and stresses in both concrete and reinforcement. Mahini and Ronagh [13] tested seven scaled-down plain / FRP-retrofitted RC exterior joints of a typical ordinary moment resisting frame under monotonic/ cyclic loads. Their test results show that the method is also effective for enhancing strength of the system. Zou et al. [14] investigated a 3-storey frame strengthened with FRP around its columns. It was noted that there was only a marginal increase in stiffness after strengthening. Slightly enhanced stiffness adds to the overall stability of the frame as stiffer columns lead to higher seismic forces. In addition, the failure mode of the frame was shifted from a column side-sway mechanism to an acceptable storey deformation level with weak beam-strong column behaviour. Mahini and Ronagh [15] and Niroomandi et al. [16] studied the peak strength of plain FRP-retrofitted joints and compared the result with those of the same frame retrofitted with steel braces. The results indicated that the FRP retrofitted RC frame is better than the steel braced retrofitted frame.

Studies were also conducted on theoretical capacity models (Ghobarah [17], Priestley et al. [18], Fave and Kim [19], Park and Mosalam [20], and Masi et al. [21]) in order to predict the strength capacity of beam-column joints and the sub-assembly failure sequence. The reliability of capacity models was also assessed by the definition of theoretical and experimental joint shear.

The extensive literature survey necessitated carrying out an experimental study on beam-column joint strengthened with repairing techniques and laminations under reversed cyclic loading. A comparison of the joint shear strength of exterior reinforced concrete beam-column joints before and after retrofit was also conducted.

The scope of present work is limited to preliminary experimental investigations aimed at comparing behaviour of exterior beam-column joints retrofitted with Hybrid FRP with banana fibres in mat form and chopped form.

With the proposed retrofit method, this research work aims to avoid joint shear failure and hence to promote beam flexural hinging.

2. Research significance

The HFRP laminations (mat banana fibre and chopped banana fibre) and GFRP wrapping are effective and economical retrofit techniques for improving seismic performance of the exterior beam-column joint. In this work, the experimental verification focuses on the load - drift envelope behaviour, ultimate load, load – drift hysteretic loops, cumulative energy dissipation, stiffness, and ductility. The theoretical validation was carried out by determining the horizontal shear force and shear strength at the joints.

3. Description of beam-column joint specimens

3.1. Analysis of RC building and design of beam-column joint

An eight storeyed reinforced concrete building located in Chennai, India, in Seismic Zone III (design acceleration coefficient (Sa/g) = 2.5 as per IS 1893 (Part 1) [22] on medium - Type II soil (Figure 1) was analysed. Each storey is 3.0 m in height. The size of the building is 20.1 m x 12.3 m. The longitudinal and transverse beams measured are 0.45 m in depth and 0.30 m in width. The live loads of 3 kN/m^2 and floor finish of 1 kN/m^2 were adopted for analysis. The M30 grade concrete (Concrete mix with characteristic compressive strength of 30 MPa) and Fe 415 grade steel (High Yield Strength Deformed steel reinforcement with yield strength of 415 MPa) were used in the design. The seismic analysis was performed using the equivalent static method as per IS 1893 (Part 1) [22]. Shear forces, bending moments, and axial forces resulting from different load combinations were determined at the beam-column interface. The following critical design forces were obtained for the section of the prototype model; axial load 4325 kN and moment 475 kN-m. The design and detailing of the beam – column joint of the prototype model were conducted based on the guidelines given in IS 456 [23] and SP 34 [24], respectively.

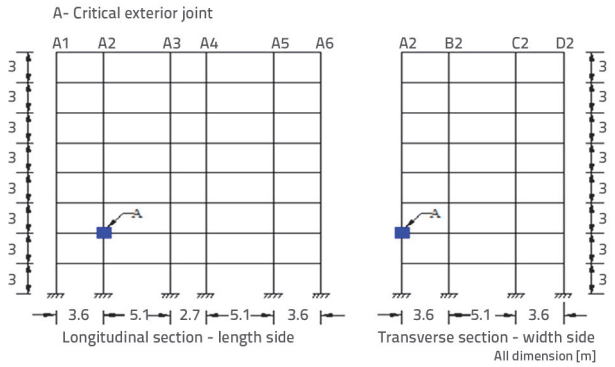

Figure 1. Sections of the prototype eight storey building

3.2. Detailing of beam-column joint scaled model

The experiment was carried out in the laboratory; the specimen size was designed according to the testing machine to the one-third scale of the prototype. The dimensions and reinforcements of the scaled model (1/3rd) following Cauchy's law of similitude (Carvalho [25]) and the beam-column joint region were detailed as per SP34 [24] (cf. Figure 2). Beam and column elements were extended between points of contraflexure (assumed to be at midspan in the beam and at midheight in the columns) where hinge connections were introduced. The height of the specimen (L_c) is taken as the distance between the point of contraflexure in the column. The dimension and the area of the scaled model with prototype are shown in Table 1.

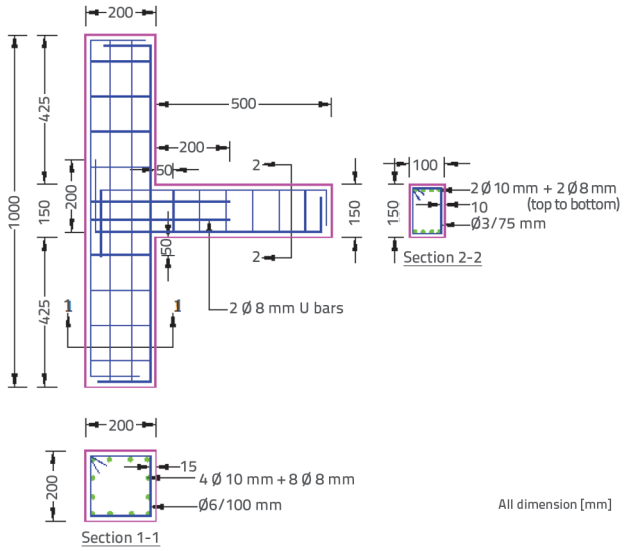

Figure 2. Reinforcement details of 1/3rd scaled model as per IS456 and SP34

3.3. Specimen description

Specimens were designated as S2BRF and S3BRF (specimen before retrofitting). The specimens after retrofitting were designated as S2ARF and S3ARF (strengthened with HFRP laminations with eight layers of GFRP wrapping). The retrofitted beam-column joint laminations are shown in Figure 3.

Table 1. Parameters of specimen

Specimen type	Column details			Beam details			Joint reinforcement
	Width [mm]	Height [mm]	Area of reinforcement [mm^2]	Width [mm]	Depth [mm]	Area of reinforcement [mm^2]	Površina armature [mm^2]
Prototype	600	600	6216	300	450	4635	904.3
Scaled model	200	200	716	100	150	515	100.5

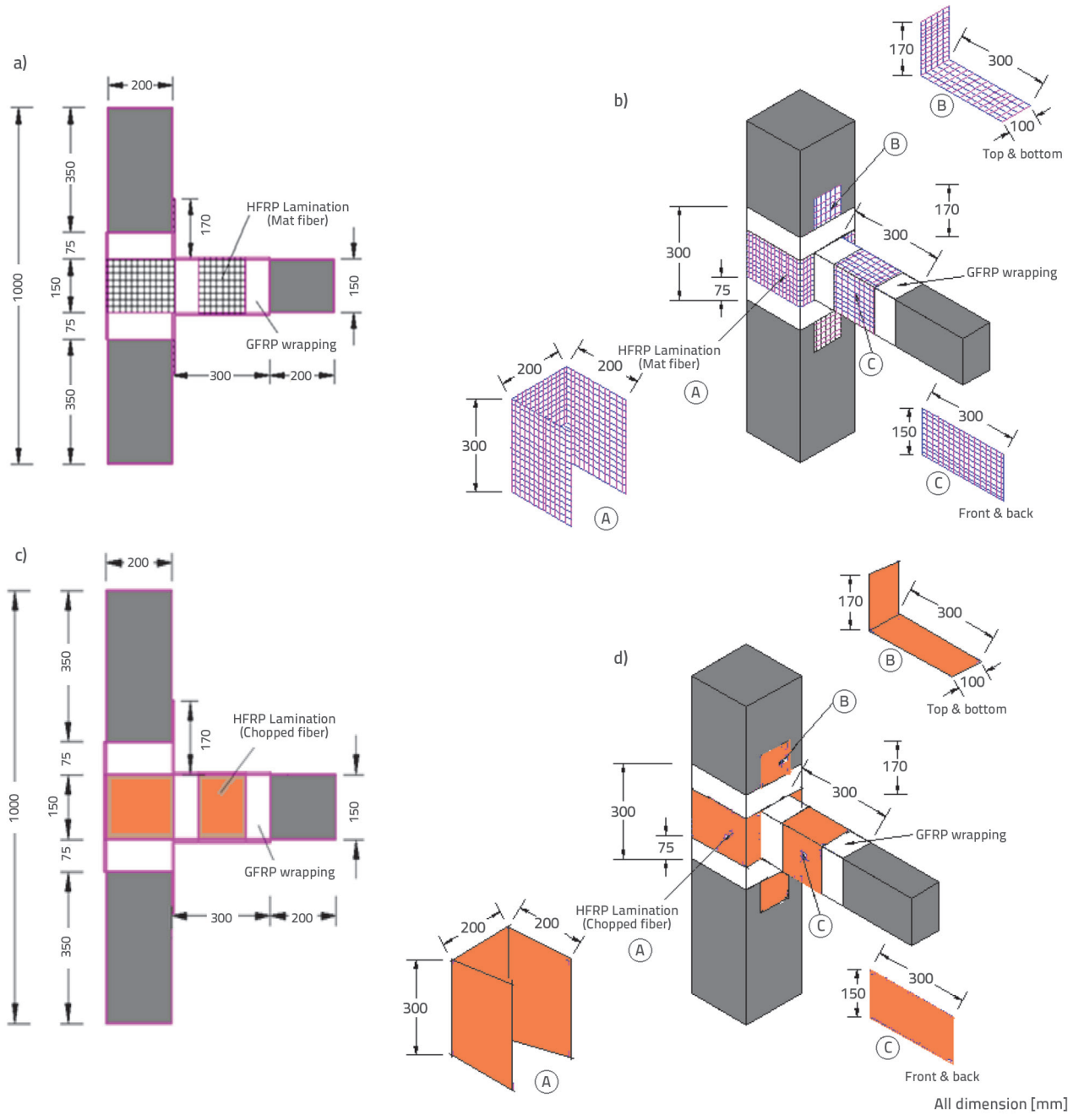

Figure 3. Strengthening with HFRP laminations and GFRP wrapping of beam-column joints: a)Front view (S2ARF); b) Isometric view (S2ARF); c) Front view (S3ARF); d) Isometric view (S3ARF)

3.4. Experimental investigation

3.4.1. Material characterisation

Concrete and steel

Ordinary Portland Cement (Grade 53) conforming to IS 12269 [26] is used. River sand and crushed granite stone of maximum size not exceeding 10 mm were used for the scaled model. M30 grade of concrete was adopted. Fe415 grade steel was used as reinforcement. The concrete mix was designed for the scaled model; the average compressive cube strength (fck) at 28 days was 39 N/mm^2. The modulus of elasticity was determined by determining the stress – strain behaviour of concrete, where secant modulus was adopted for the model (E_c = 29.7 GPa).

Retrofitting materials

Retrofitting of the exterior beam-column joint was carried out by removing and replacing concrete in the regions of damaged joints. Special attention was given to ensuring a good bond between the new and existing concrete during the process of retrofitting. The

Table 2. Mechanical properties of strengthening laminates

Strengthening system	Type of fibre	Tensile strength [MPa]	Elastic modulus [GPa]	Ultimate strain [%]	Thickness [mm]
First system	Mat form	67	12.5	6	4
Second system	Chopped form	45	13.13	5	4

damaged region was replaced by new concrete. The strength of the mix which was used to repair the joint had to have the same strength as the existing concrete (39 MPa). The maximum size of aggregate to be used for making repair concrete was less than 10 mm. The mix proportion was 1:1.51:2.53 by weight, and the water - cement ratio was 0.45. Forging slag was used (20 %) as partial replacement of fine aggregate and an elastomer material SBR (Styrene butadiene rubber) was used in such proportion (20 %) by volume of water that improves bonding with the cement paste. Super-plasticizer (1 %) was also used as a water reducing agent to get the required workability. Epoxy resin (3:1) was used as a bonding layer between the existing concrete and new concrete and it also ensured that most of the visible cracks were fully filled with epoxy resin.

Hybrid fibre reinforced polymer (HFRP) laminate

Two types of HFRP laminate strengthening systems were used in this research. The first system consisted of banana fibre in mat form (bidirectional) with glass fibre (bidirectional 610g/m^2). The second system consisted of banana fibre in chopped form (12 mm length and 100-125 microns diameter) as reinforcement and epoxy as matrix. The method of fabrication adopted was the resin transfer method. The liquid resin mix comprising the epoxy resin (Araldite LY 556) and hardener (HY 951) in the proportion of 10:1 by weight was used for both lamination systems. For the first system (Mat form) the volume fraction was 60 % hybrid reinforcement and 40 % matrix, whereas for the second system (chopped form) the volume fraction was 48 % hybrid reinforcement and 52 % matrix. Detailed characteristics of the two types of HFRP laminate and the epoxy resin used in this work are given in Table 2.

Glass fibre reinforced polymer (GFRP)

For strengthening the two specimens (S2ARF and S3ARF) by GFRP wrapping, the thickness must be at least 35 % greater than that of the sheet thickness to prevent rupture (Granata and Parvin [27]). Eight layers of GFRP (total thickness of 1 mm) are utilized for wrapping both specimens. The tensile strength, modulus of elasticity, and ultimate strain are 81 MPa, 20 GPa, and 4 %, respectively.

Adhesive

The adhesive used in bonding laminate to concrete was Sikadur 330 2 mm in thickness. The resin and hardener were mixed in the ratio 3: l (by weight). A uniform mid-grey colour indicates sufficient mixing of the white resin and black hardener with silica used as filler. 2mm thickness of the Sikadur 330 was used in the present work. The specimens were cured for 7 days before testing. The average strength and modulus were 28.4MPa and 8.6 GPa, respectively.

3.4.2.Retrofitting procedure

The preparation of adhesion surfaces is essential before the lamination could be bonded to concrete. Grit blasting was conducted on damaged concrete surfaces with 180-mesh alumina at an average pressure of 207 kPa (30 psi) in a pressure-fed re-circulating machine, and then clean air was blown to remove dust. The adhesive was applied to both surfaces in order to prevent formation of air bubbles by the spread of adhesive from one surface to the other. Ballotini (Glass spheres) was used to get the desired glue line thickness of 2 mm. The bonding pressure was applied by weights to achieve a uniform distribution of load over the plan area of each lamination as shown in Figure 4.

3.4.3. Test setup

The exterior beam-column joint specimens (scaled to 1/3) were tested in the well–equipped set-up of 200 Tonne capacity in a steel loading frame in Structural Dynamic Laboratory, Division of Structural Engineering, Anna University, Chennai, India. To stimulate the test model, the column bottom end was provided with hinged support and the column top end was provided with roller support. 10 % of constant axial load (5 tonnes) was applied at the column top end as this will in turn allow the joint to dissipate higher energy during cyclic loading. The load was kept constant during the entire loading procedure for all specimens. The steel support base was properly fixed to the strong reaction floor. Load cells and dial gauges were used to record the load and displacement of specimens. Two 10 tonne hydraulic jacks were used to apply the reverse cyclic loading at the top and bottom ends of the beams. Displacement control was adopted for the model. The loading protocol considered a series of three cycles at increasing levels of drift. Both the dial gauges and load cells were instrumented at a distance of 50mm from the tip of the beam. The dial gauge was used to control that displacement occurs according to the loading protocol. The corresponding loads were noted using a load cell (Push and Pull). The experimental test setup presented in Figure 5 shows: a) test setup in laboratory-S2ARF and b) test setup in laboratory-S3ARF. The position of monitoring instrument is shown in Figure 6.

Figure 4. Before and after specimen retrofit: a) Before retrofit (Levelling the surface (left), Adhesive (right)); b) After Retrofit (S2ARF Retrofit (left), S3ARF Retrofit (right))

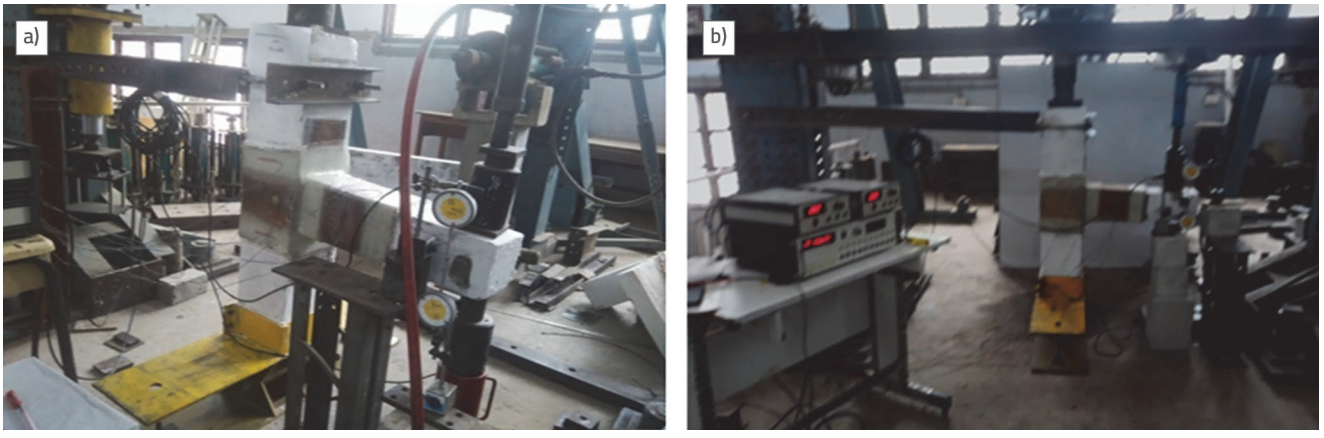

Figure 5 . Test setup in laborator: a) specimen S2ARF; b) specimen S3ARF

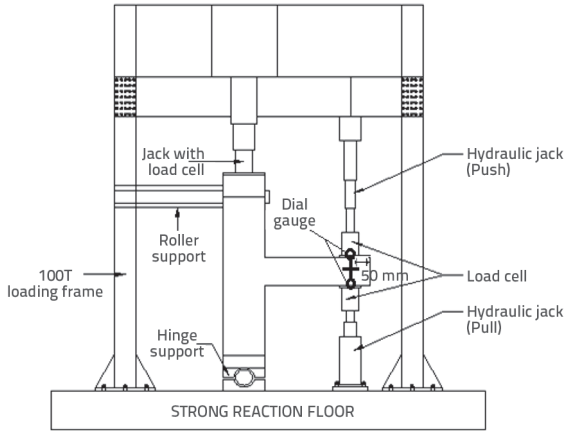

Figure 6. Schematic diagram of test set-up

Figure 7 shows a typical loading protocol (Pampanin et al. [28]) used for all specimens.

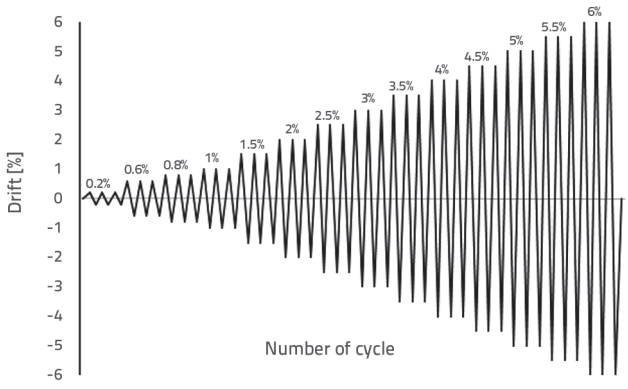

Figure 7. Loading protocol

4. Experimental results and discussion

Test results obtained before retrofitting and after retrofitting are described in this section.

4.1. Ultimate Load

The ultimate load measured from the experimental investigation for the specimens before and after retrofitting for push and pull direction of loading is shown in Table 3.

Table 3. Comparison of ultimate load carrying capacity

Specimens	Ultimate load [kN]		
	Push	Pull	Average
S2BRF	40	38	39
S2ARF	63,11	62	62,56
S3BRF	40,45	37,6	39,03
S3ARF	66,75	64	65,38

The maximum ultimate load was observed for S3ARF specimen and was found to be 67.5 % higher than S3BRF specimen. S3ARF specimen showed higher ultimate load compared to S2ARF specimen and the percentage increase is 4.5 %.

4.2. Load – Drift Hysteretic loops

The load - drift hysteresis loop was plotted for both systems of laminations, as shown in figures 8 and 9. The pinching effect induced due to bond stress-slip and shear sliding was also considered in hysteretic loops. For retrofitted specimens, the areas of hysteresis loops gradually increased as the drift cycle increased, with better energy dissipating capacity for the S2ARF specimen compared to S3ARF specimen. The load – drift envelope curve is shown in Figure 10.

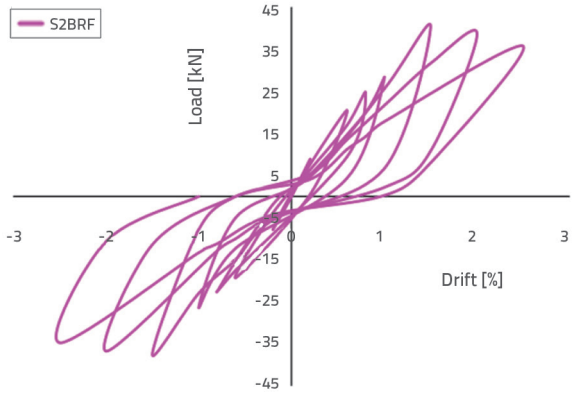

Figure 8. Load – drift hysteresis loop for un-retrofitted specimen (S2BRF)

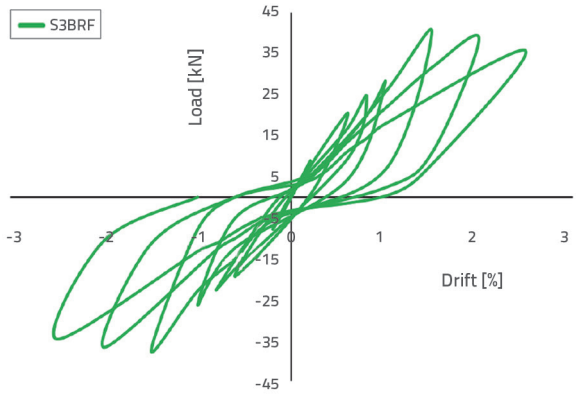

Figure 9. Load – drift hysteresis loop for un-retrofitted specimen (S3BRF)

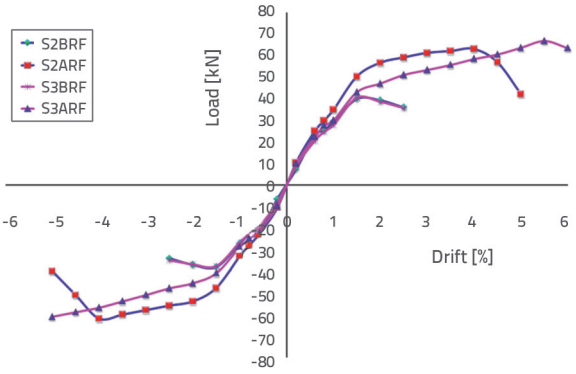

Figure 10. Load – drift of envelopes curves

4.3. Energy dissipation

Energy dissipation capacity is an important criterion for assessing performance of a component when subjected to seismic loading, with the assessment depending mainly on the rates of stiffness degradation and strength degradation in each cycle during hysteresis response.

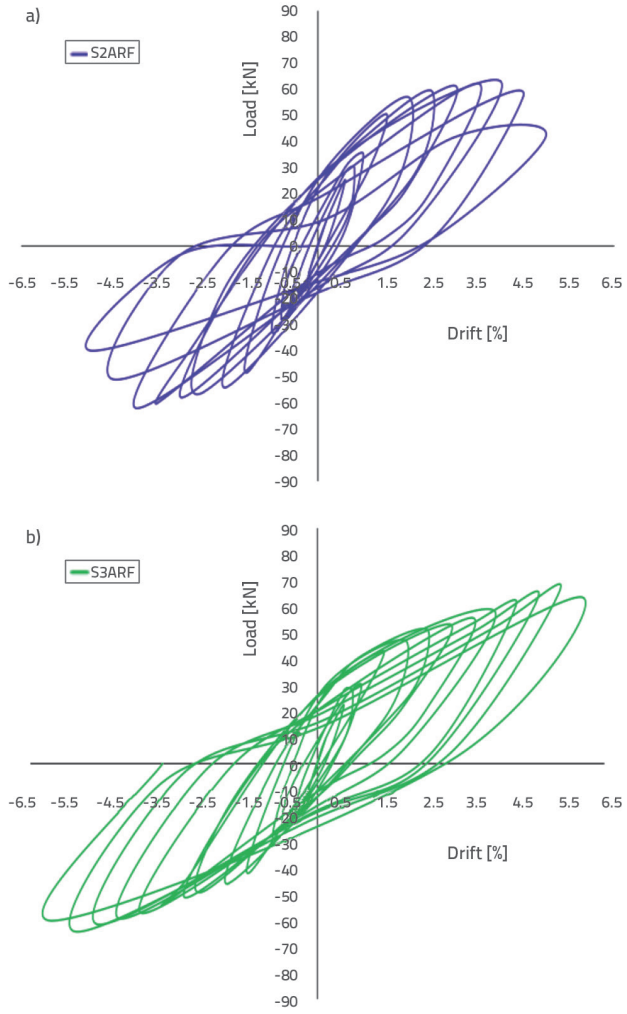

Figure 11. Load – drift hysteresis loop for retrofitted specimen

The cumulative energy dissipation of the specimens obtained from the experiments is shown in Figure 11. The energy dissipation of S2ARF and S3ARF specimens was found to be by 68.3 % and 44.4 % higher compared to that of S2BRF and S3BRF specimens, respectively, at 2.5 % drift ratio, as shown in Figure 12. At higher drift ratios, the specimens with higher joint shear stresses showed higher energy dissipation. An increase in joint shear stress resulted in greater damage to the joint, which led to greater energy dissipation.

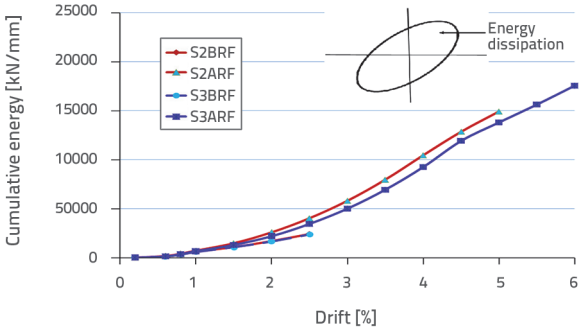

Figure 12. Cumulative energy dissipation

4.4. Stiffness Degradation

The stiffness of beam-column joints is estimated by using the slope of the peak-to-peak line for each loop at each drift ratio (ACI 318 [29]). The structure has an enhanced ductility due to a lower rate of degradation. At a 2.5 % drift ratio, the stiffness of strengthened S2ARF specimens is by 63.3 % higher compared to that of S2BRF specimens, as shown in Figure 13.

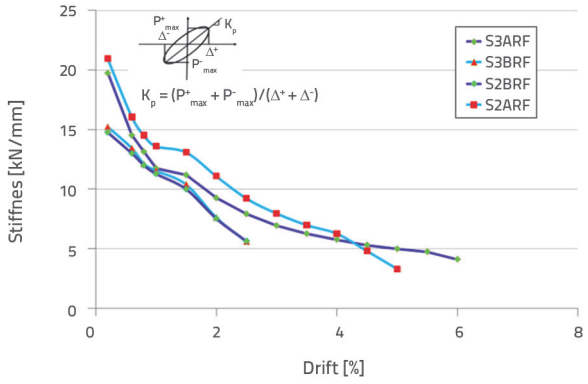

Figure 13. Stiffness curve

The stiffness of a structure is its resistance to deformation and the strengthened S2ARF specimens show greater stiffness than the S3ARF specimens, as shown in Table 4 and Figure 14.

Table 4. Comparison of secant stiffness

Specimens	Yield displacement [mm]		Secant stiffness [kN/mm]		Secant stiffness [kN/mm]
	Push dy^+	Pull dy^-	Push	Pull	
S2BRF	1.6	1.47	8.78	8.6	17.38
S2ARF	2.5	2.3	9.26	9.2	18.46
S3BRF	1.6	1.47	8.78	8.6	17.38
S3ARF	3.0	2.78	8.9	9.2	18.1

Table 5. Comparison of displacement ductility

Specimens	Yield displacement [mm]			Ultimate displacement [mm]			Ductility factor
	Push	Pull	Average	Push	Pull	Average	
S2BRF	4.73	4.53	4.63	7.5	7.5	7.5	1.619
S2ARF	6.93	6.81	6.87	20.1	19.93	20.01	2.91
S3BRF	4.65	4.38	4.52	7.5	7.5	7.5	1.66
S3ARF	10.,06	9.,65	9.86	27.5	27.,5	27.5	2.789

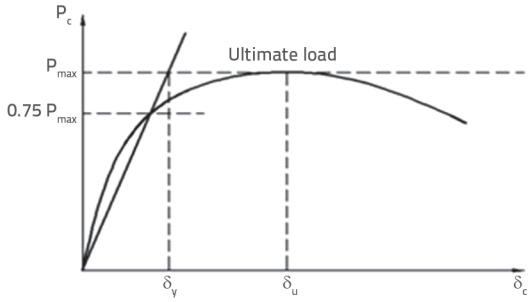

Figure 14. Secant stiffness

4.5. Ductility

The displacement ductility is defined as the ratio of the ultimate displacement (δ_u) to the yield displacement (δ_y). Yield load (P_y) and δ_y are determined as per Figure 15.

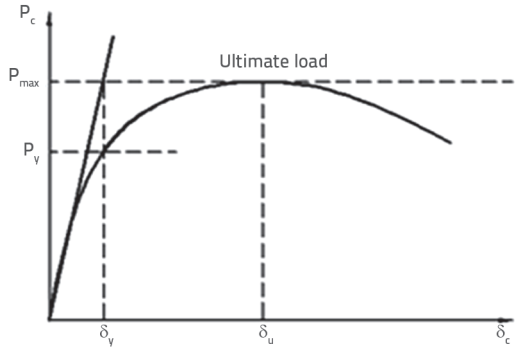

Figure 15. Displacement ductility

P_{max} and δ_u are the peak load and the corresponding displacement on the load-displacement curve, respectively. The displacement ductility of the specimens indicates that retrofitted specimens behave in a ductile manner for two types of systems. The enhancement in displacement ductility for S2ARF was observed to be by 79.74 % higher compared to S2BRF specimen. For S3ARF the percentage of increase is 68 % only, as given in Table 5. The yield displacement is computed by plotting the load-drift envelope curve from hysteretic loops based on the equivalent elastic-plastic yield model. The ultimate displacement is calculated as the point of maximum force that the specimen could withstand based on peak load, [30].

4.6. Failure observation

Specimens S2BRF and S2ARF

In S2BRF specimen, a crack was initiated from the column face towards the beam during the third cycle of loading (0.8 % downward drift). In the fourth and fifth cycles of loading (1 % and 1.5 % of drift), it was observed that a series of flexural and flexural–shear cracks were formed along the beam length. These cracks grew wider during the sixth and seventh cycles of loading (2 % and 2.5 % of drift) (Figure 16).

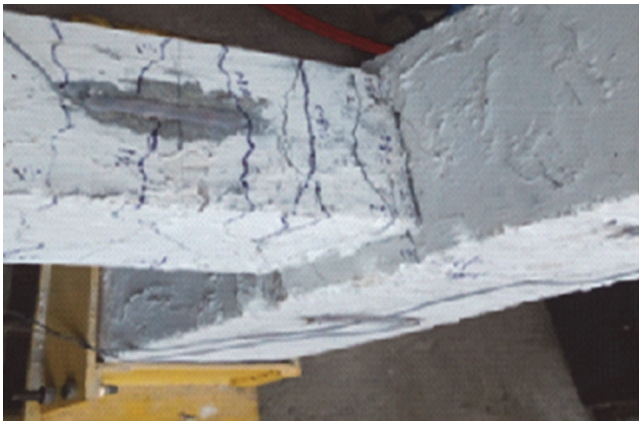

Figure 16. Crack pattern of specimen (S2BRF)

For S2ARF specimen, cracks were initiated only during the fourth cycle of loading (1 % drift) and were observed to further develop

during the fifth cycle of loading (1.5 % drift). Furthermore, shear cracks were developed at beam top away from the retrofitted area. No further cracks were developed in this region. As the drift was gradually increased there were no signs of a crack, de-bonding, and de-lamination up to the eighth cycle of loading (3 % drift). The signs of rupture were observed at the top of the column wrap located at the beam-column junction, during the ninth cycle of loading (3.5 % drift). The development of rupture, along with peeling of the column wrap, was observed at the edge nearer to the beam during the tenth cycle of loading (4 % drift). Also, initial de-bonding was observed at the same location of rupture at 4 % drift. During the eleventh cycle of loading (4.5 % drift), full de-bonding with severe rupture developed at the same location. The specimen was found to attain full failure at beam-column joint during the twelfth cycle of loading (5 % drift) (Figure 17).

Figure 17. Crack pattern of S2ARF at 5 % drift

Figure 18. Crack pattern of specimen (S3BRF)

Specimens S3BRF and S3ARF

In S3BRF specimen, during downward drift of the third cycle (0.8 % drift), a crack was initiated at the column face and propagated towards the beam during the third cycle of loading (0.8 % drift). The flexural and flexural–shear cracks developed during the fourth and fifth cycle of loading (1 % and 1.5 % drifts), respectively. Cracks become wider during the sixth and seventh cycles of loading (2 % and 2.5 % of drift), as shown in Figure 18.

In S3ARF specimen, as the drift gradually increased, there were no signs of a crack in concrete. The signs of rupture were observed at the top of the column wrap located at the beam-column junction, during the eighth cycle of loading (3.0 % drift). Furthermore, development of rupture was observed along with peeling of the column wrap at the edge nearer to the beam, and initial de-bonding started at the beam-column connection during the ninth cycle of loading (3.5 % drift). Development of deep de-bonding occurred at the connection at the tenth cycle of loading (4 % drift). During the eleventh cycle of loading (4.5 % drift), new de-bonding occurred in the middle of the bottom lamination, at the bottom of the beam, and at the beam-column connection point. De-bonding developed deeper and so the lamination split further from the concrete surface. Complete failure of the beam–column joint specimen occurred during the fourteenth cycle of loading (6 % drift), as shown in Figure 19: a) failure at 5 %, b) failure at 6 %, c) Complete failure at 6 %.

5. Theoretical analysis

In framed structures, large shear force is generated in the exterior joint region due to seismic force. Some of the internal forces, generated in the concrete will combine to develop a diagonal strut. The truss mechanism depends on the effectiveness of the bond between the concrete and the steel bars (beam and column bars). The transverse reinforcement in the joint confines the concrete diagonal strut in the joint core and contributes to an increase in joint strength. Forces that developed at the proposed beam-column joint are shown in Figure 20. Joint shear forces generated due to external forces are shown in Figure 21.

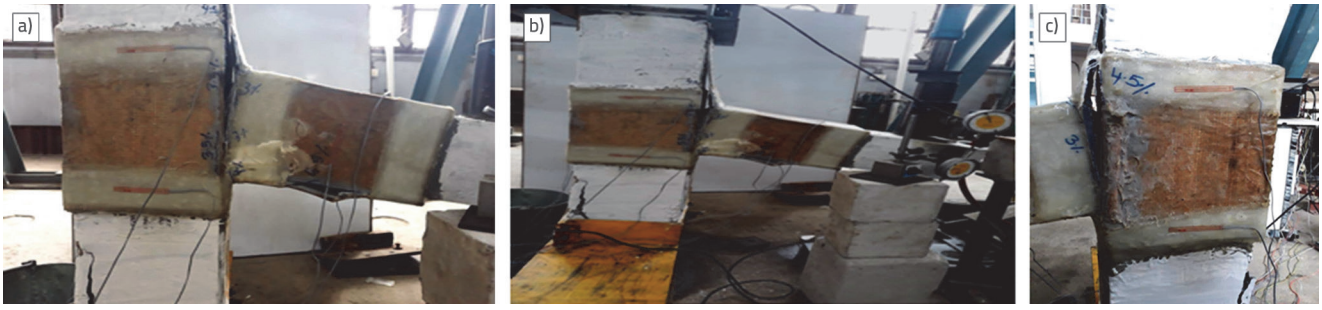

Figure 19. Crack pattern of S3ARF: a) failure at 5 %; b) failure at 6 %; c) complete failure at 6 %

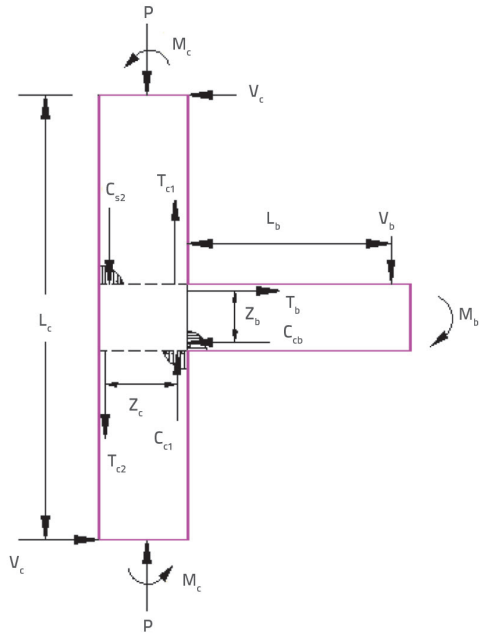

Figure 20. External and internal forces in beam and column

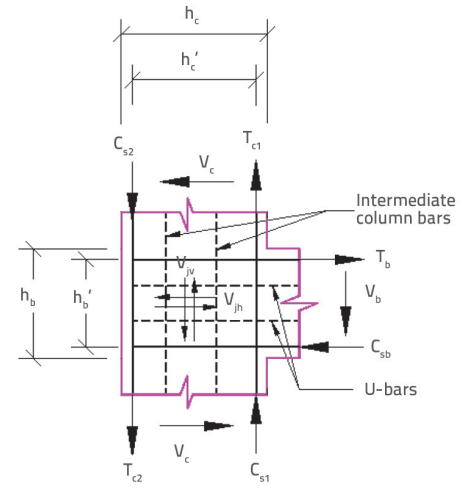

Figure 21. Joint horizontal and vertical shear forces

The labels in Figures 20 and 21 have the following meanings:

C_{cb}, C_{c1}, C_{c2} - compressive force in the beam and the column concrete,
C_{sb}, C_{s1}, C_{s2} - compressive force in the beam and the column reinforcement,
h_b, L_b - depth and the length of the beam concrete,
h_c, L_c - depth and the height of the column concrete,
h_b', h_c' - depth of the beam and the column reinforcement,
M_b, M_c - moment in the beam and the column
P - axial load,
T_b, T_{c1}, T_{c2} - tensile force in beam and the column reinforcement,
V_b i V_c - vertical and horizontal shear force of the beam and the column,
V_{jv}, V_{jh} - vertical and horizontal joint shear forces,
Z_b, Z_c - lever arm of the beam and the column.

5.1. Joint shear force

The maximum horizontal shear force at the joint (V_{jh}) from theoretical analysis can be calculated using the equilibrium of forces acting at the connection just before failure, as shown in Eq. (1).

$$V_{jh} = T_b - V_c \quad (1)$$

$$T_b = \alpha A_s f_y \quad (2)$$

where α - stress multiplier for longitudinal reinforcement at a joint-member interface.

$$T_b = \frac{M_b}{Z_b} = \frac{V_b - L_b}{Z_b} \quad (3)$$

Hence (V_b) from theoretical analysis is determined from Eq. (3). The equilibrium of external forces, from which V_c (theoretical study) can be computed, is given in Eq. (4). Further maximum horizontal shear force from theoretical analysis (V_{jh}) is obtained from Eq. (1).

$$V_C = \frac{V_b\left(L_b + 0{,}5h_C\right)}{L_C} \quad (4)$$

For the HFRP retrofitted specimens, the joint shear force ($V_{jh\ retrofitted}$), corresponding to the maximum beam flexural capacity, can be calculated by assuming that the tensile force in the longitudinal reinforcement of the beam (T_b) does not change in the retrofitted specimens, as shown in Eq. (4).
For computing the maximum horizontal shear force from the experimental investigation (V_{jh}), vertical shear force (V_b) of the beam has been taken as the experimental ultimate load and the horizontal shear force (V_c) in the column is computed from Eq. (4). Hence, (V_{jh}) is calculated using Eq. (1). Similarly, $V_{jh\ retrofitted}$ is computed from Eq. (5).

$$V_{jh,\ retrofitted} = T_b + T_{HFTP} - V_c \quad (5)$$

where:
$T_{HFRP} = \varepsilon_f A_f E_f$ - tensile force in the hybrid fibre reinforced polymer
ε_f - strain in the HFRP
A_f - cross section area of the HFRP
E_f - elasticity of the HFRP.

5.2. Joint shear strength

The design ultimate shear capacity of joint before failure (V_n), from experimental and theoretical study, can be computed using Eq. (6).

$$V_n = V_c + V_s, \text{ and } V_s = 0{,}87 f_y A_s \quad (6)$$

where:

V_s - design link shear force resistance
V_c - design shear force resistance of concrete in a joint
f_y - yield stress of reinforcement
A_s - cross section area of the reinforcement.

While for retrofitted joints, the total shear resistance ($V_{n,\ retrofitted}$) consists of the concrete resistance, the resistance of the ties and the resistance provided by the composite lamination, is given by Eq. (7).

$$V_{n,\ retrofitted} = V_c + V_s + V_{HFRP} \quad (7)$$

$$V_{HFRP} = 0{,}9\varepsilon f_e E_f \rho_f A_j \quad (8)$$

where:
V_{HFRP} - design shear force resistance of hybrid fibre reinforced polymer in a joint (Hadi and Tran [31])
ρ_f - FRP reinforcement ratio
ε_{fe} - effective strain level in FRP reinforcement
E_f - elastic modulus of (FRP).

5.3. Design guidelines

The increased flexural strength of the section (M_b), calculated as per ACI-ASCE Committee 352 [32]

$$M_b = A_s \alpha f_y (d - a/2) \quad (9)$$

where:
d - distance from extreme compression fibre to centroid of tension reinforcement
b - width of the concrete beam
a - depth of equivalent rectangular compression block
α - stress multiplier for longitudinal reinforcement at joint-member interface.

$$a = \frac{A_S \alpha f_y}{0{,}85 f_{ck} b} \quad (10)$$

The shear in column (V_c) is calculated based on the nominal flexural strength of the section

$$V_c = \frac{M_b}{L_c} \quad (11)$$

where L_c - the height of the column.

The horizontal shear force ($V_{jh\ ACI}$) can be obtained from Eq. (1). ACI-440.2R-08 [33] requirements for the nominal flexural strength of the joint retrofitted (M_n) should be satisfied as per Eqs. (12) to (16)

$$M_n = M_{ns} + \Psi_f M_{nf} \quad (12)$$

where:
M_{ns} - contribution of steel reinforcement to the nominal flexural strength
M_{nf} - contribution of HFRP reinforcement to the nominal flexural strength
A_f - the area of external HFRP reinforcement
Ψ_f - FRP strength reduction factor (0.95).

Flexural strength of the beam is calculated using sectional analysis as presented in Figure 22.
β - ratio of depth of equivalent rectangular stress block to non-linear distribution of stress
c - distance from extreme compression fibre to the neutral axis
b_f - effective width of the FRP flexural reinforcement,
ε_c, ε_{sc} - reffective compressive strain level in the concrete and the steel,
ε_{ct}, ε_{st} ε_f - effective tensile strain level in the concrete, steel and FRP.

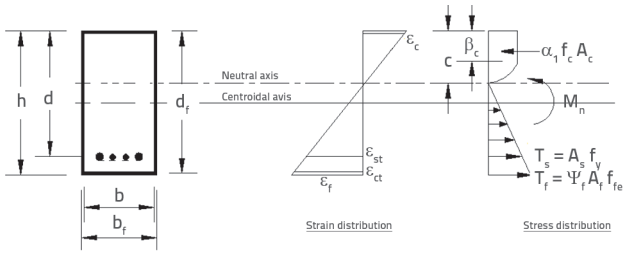

Figure 22. Sectional analysis of beam strengthened with FRP

$$M_n = A_s f_y \left(d - \frac{\beta c}{2} \right) + \Psi_f A_f f_{fe} \left(d_f - \frac{\beta_c}{2} \right) \quad (13)$$

$$\beta = \frac{4\varepsilon_c' - \varepsilon_c}{6\varepsilon_c' - 2\varepsilon_c} \quad (14)$$

ε'_c = 1,7f_c / E_c ε'_c strain corresponding to f_c, and E_c is elastic modulus of concrete.

$$c = \frac{A_s f_y + A_f f_{fe}}{\alpha_1 f_c \beta_b} \quad (15)$$

where α_1 multiplier on f_c to determine intensity of an equivalent rectangular stress distribution for concrete, and f_{fe} effective stress in the FRP stress level attained at section failure.

$$\alpha_1 = \frac{3\varepsilon_c' \varepsilon_c - \varepsilon_c^2}{3\beta \varepsilon_c'^2} \quad (16)$$

The maximum tensile force (T_n) that can be carried by the horizontal FRP layer along the beam can be calculated as per the guidelines.

$$T_n = \frac{M_n}{d_f} \quad (17)$$

where d_f effective depth of the HFRP flexural reinforcement.

$$V_{jh,\ retrofitted} = T_b + T_n + V_c \quad (18)$$

T_b and V_c can be determined from Eq. (2) and Eq. (4)

Table 6. Experimental and theoretical evaluation of joint forces

System	Specimen	Joint force [kN]							
		Experimental				Theoretical			
		V_{jh} [Eq. (1)]	$V_{jh\ retrofit}$ [Eq. (5)]	V_n [Eq. (6)]	$V_{n\ retrofit}$ [Eq. (7)]	V_{jh} [Eq. (1)]	$V_{jh\ retrofit}$ [Eq. (5)]	V_n [Eq. (6)]	$V_{n\ retrofit}$ [Eq. (7)]
First system	S2BRF	101.6	-	102.2	-	106.7	-	217.4	-
	S2ARF	-	176.1	-	177.2	-	195.3	-	240.0
Second system	S3BRF	101.6	-	102.2		106.7	-	217.4	-
	S3ARF	-	165.9	-	169.9	-	186.8	-	241.9

Table 7. Comparison of experimental and theoretical evaluation of joint forces

System	Specimen	ACI		Joint shear force ratio	
		V_{jh} [Eq. (1)]	$V_{jh\ retrofit}$ [Eq. (18)]	$\frac{V_{jh}^{exp}}{V_{jf}^{ACI}}$	$\frac{V_{jh}^{Theo}}{V_{jf}^{ACI}}$
First system	S2BRF	109.4	-	0.93	0.97
	S2ARF	-	221.0	0.80	0.88
Second system	S3BRF	109.4	-	0.93	0.97
		-	217.6	0.76	0.86

6. Comparison of experimental and theoretical results

The horizontal joint shear force, shear strength, and joint shear ratio, were evaluated for the experimental and theoretical study in Table 6. The detailed comparison is given in Table 7.

It can be observed from Table 7 that a reasonably good agreement exists between theoretical and experimental values of V_{jh}. The ACI guidelines values are higher particularly for S2ARF and S3ARF specimens.

Note: V_{jh}^{exp} is the experimental joint shear force, V_{jh}^{Theo} is the theoretical joint shear force, and V_{jh}^{ACI} is the ACI guidelines joint shear force. V_n^{exp} is the experimental joint shear strength, V_n^{Theo} is the theoretical joint shear strength, and V_n^{ACI} is the ACI design guidelines joint shear strength.

7. Conclusions

The following conclusions can be made based on the experimental and theoretical analysis:

- The ultimate load was observed to be matching (< 5 % variation) for both types of retrofitted specimens (S2ARF and S3ARF). The experimental ultimate load carrying capacity for retrofitted specimen (S2ARF) is by 4.5 % higher compared to S3ARF specimen. The load carrying capacity of S2ARF was observed to be by 25.7 % higher than that of S2BRF whereas, for S3ARF, the variation is within 6.3 % at 2.5 % drift level.
- A slight increase in the displacement ductility was observed for S2ARF (< 5 %) compared to S3ARF in the retrofitted specimens. It was found that S2ARF specimen had 4.3 % more than the S3ARF. However, there is an enormous increase in the displacement ductility for S2ARF (79.7 %) and S3ARF (68 %) when compared to S2BRF and S3BRF.
- Spindle-shaped hysteretic loops exhibit large energy dissipation capacity for both types of retrofitting systems (S2ARF and S3ARF). The experimental results were compared with the backbone envelope curve of hysteretic load – drift loops (ultimate load and stiffness)
- The stiffness shows an increase of 63.3 % for S2ARF specimen compared to S2BRF specimen, and S3ARF is by 41.4 % greater than S3BRF at a 2.5 % drift level. Thus the variation is 16.3 % compared to S2ARF and S3ARF from experimental investigation.
- The un-retrofitted specimen develops diagonal shear failure at the top and bottom of the beam that contributes to the failure of the specimen when tested under reverse cyclic loading at a 2.5 % drift. However, the retrofitted specimen exhibited cracking at the edge, creep at the GFRP wrapping, rupture of HFRP lamination, and suffered bent reinforcement when retested under reverse cyclic loading at a 5 % drift.
- The joint shear force and shear strength based on available design guidelines (ACI) were compared with the experimental value of joint shear strength. Good correlation was observed between the theoretical and experimental results.
- Comparing the seismic performance of the HFRP retrofitted beam-column joints with different strengthening retrofitting methods, it is concluded that both retrofitting schemes have the comparable capability to increase the ductility factor and strength. In specimen S2ARF, the use of HFRP lamination (Mat banana fibre) prevents de-bonding from the concrete surface by up to

5 % drift ratio. The HFRP reached a strain up to ultimate strain without failure in both tension and compression. The retrofitted joints exhibited 67.5 % higher loading capacity and dissipated four times the energy dissipated by the un-retrofitted specimens (S2BRF).

Acknowledgments

Financial assistance provided by the University Grant Commission through Rajiv Gandhi National Fellowship for supporting the Ph.D. scholarship is greatly acknowledged by the authors.

REFERENCES

[1] Kaushik, B.H., Jain, S.K.: Impact of Great December 26, 2004, Sumatra Earthquake and Tsunami on Structures in Port Blair. Journal of Performance of Constructed Facilities, 21 (2007) 2, pp.128-142, https://doi.org/10.1061/ (ASCE) 0887-3828 (2007) 21:2 (128)

[2] Saatcioglu, M., Ghobarah, A., Nistor, I.C.: Effects of December 26, 2004, Sumatra earthquake and tsunami on physical infrastructure, Journal of Earthquake Technology, 42 (2005) 4, pp.79-94, http://home.iitk.ac.in/~vinaykg/Iset457.pdf

[3] Ghobarah, A., Said, A.: Shear strengthening of the beam-column joints, Engineering of Structures, 24 (2002), pp. 881-888, https://doi.org/10.1016/S0141-0296(02)00026-3

[4] Ozcan, O., Binici, B., Ozcebe, G.: Improving seismic performance of deficient reinforced concrete columns using carbon fibre-reinforced polymers, Engineering Structures, 30 (2008) 1, pp.1632-1646.https://doi.org/10.1016/j.engstruct.2007.10.013

[5] Antonopoulos, C., Triantafillou, T.C.: Experimental investigation of FRP-strengthened RC beam-column joints, Journal of Composites for Construction, 7 (2003) 1, pp. 39-49, https://doi.org/10.1061/(ASCE)1090-0268(2003)7:1(39)

[6] Attari, N., Amziane, S., Chemrouk, M.: Efficiency of beam-column joint strengthened by FRP laminates. Advance Composite Materials,19 (2010), pp.171-183, https://doi.org/10.1163/092430409X12605406698192

[7] Engindeniz, M., Kahn, L.F., Zureick, A.H.: Repair and strengthening of reinforced concrete beam-column joints: State of the art. ACI Structural Journal, 102 (2005) 2, pp. 187-197.

[8] Mosallam, A.S., Banerjee, S.: Shear enhancement of reinforced concrete beams strengthened with FRP composite laminates. Composites Part B: Engineering, 38 (2007), pp.781-793, https://doi.org/10.1016/j.compositesb.2006.10.002

[9] Parvin, A., Granata, P.: Investigation of the effects of fibre composites at concrete joints. Composites Part B: Engineering, 31 (2000), pp.499-509, https://doi.org/10.1016/S1359-8368(99)00046-3

[10] Said, A.M., Nehd, I.M.L.: Use of FRP for RC frames in seismic zones: Part I. Evaluation of FRP beam-column joint rehabilitation techniques, Applied Composite Materials, 11 (2004), pp.205-226, https://link.springer.com/content/pdf/10.1023%2FB%3AACMA.0000035462.41572.7a.pdf

[11] Mukherjee, A., Joshi, M.: FRPC reinforced concrete beam-column joints under cyclic excitation. Composite Structures, 70 (2005) 9, pp. 185-199, https://doi.org/10.1016/j.compstruct.2004.08.022

[12] Parvin, A., Wu, S.H.: Ply angle effect on fibre composite wrapped reinforced concrete beam-column connections under combined axial and cyclic loads. Compoite Structures, 82 (2008) 4, pp.532-538, https://doi.org/10.1016/j.compstruct.2007.02.004

[13] Mahini, S.S., Ronagh, H.R.: Strength and ductility of FRP web-bonded RC beams for the assessment of retrofitted beam-column joints. Composite Structures, 9 (2010) 6, pp.1325-1332, https://doi.org/10.1016/j.compstruct.2009.09.006

[14] Zou, X.K., Teng, J.G., Lorenzis, L.D., Xu, S. H.: Optimal performance-based design of FRP jackets for seismic retrofit of reinforced concrete frames. Composites Part B: Engineering, 38 (2007), pp.584-597, https://doi.org/10.1016/j.compositesb.2006.07.016

[15] Mahini, S.S., Ronagh, H.R.: Web-bonded FRPs for the relocation of plastic hinges away from the column face in exterior RC joints, Composite Structures, 93 (2011), pp.2460-2472, https://doi.org/10.1016/j.compstruct.2011.04.002

[16] Niroomandi, A., Maheri, A., Maheri, M.R., Mahini, S.S.: Seismic performance of ordinary RC frames retrofitted at joints by FRP sheets. Engineering Structures, 32 (2010) 8, pp.2326-2336, https://doi.org/10.1016/j.engstruct.2010.04.008

[17] Ghobarah, A., El-Amoury, T.: Seismic rehabilitation of deficient exterior concrete frame joints. Journal of Composites for Construction, (2005), pp. 408-416. https://doi.org/10.1061/(ASCE)1090-0268(2005)9:5(408)

[18] Priestley, M.J.N.: Displacement-based seismic assessment of reinforced concrete buildings. Journal of Earthquake Engineering, 1 (1997) 1, pp.157-192.

[19] Fave, J.M.L, Kim, J.: Joint shear behaviour prediction for RC beam-column connections. International Journal of Concrete Structures and Materials, 5 (2011) 1, pp. 57-64, https://doi.org/10.4334/IJCSM.2011.5.1.057

[20] Park, S., Mosalam, K.M.: Parameters for shear strength prediction of exterior beam-column joints without transverse reinforcement. Engineering Structures, 36 (2012), pp.198-209, https://doi.org/10.1016/j.engstruct.2011.11.017

[21] Masi, G., Santarsiero, G.P., Lignola, G.M., Verderame, G.M.: Study of the seismic behaviour of external RC beam-column joint through experimental tests and numerical simulation. Engineering Structures. 52 (2013), pp.207-219, https://doi.org/10.1016/j.engstruct.2013.02.023

[22] IS 1893 (Part 1): 2002-Indian Standard Criteria for Earthquake Resistant Design of Structures, Part 1: General Provisions and Buildings (Fifth Revision), BureauofIndian Standards, NewDelhi, https://law.resource.org/pub/in/bis/S03/is.1893.1.2002.pdf

[23] IS 456: 2000-Indian Standard Plain and Reinforced Concrete-Code of Practice (Fourth Revision), Bureau of Indian Standards, New Delhi, http://www.iitk.ac.in/ce/test/IS-codes/is.456.2000.pdf

[24] SP 34: 1987-Handbook on Concrete Reinforcement and Detailing, Bureau of Indian Standards, New Delhi, https://www.uiet.co.in/downloads/20140911095221- sp.34.1987 %20Structural %20Designing %20Practice.pdf

[25] Carvalho, E.C.: Invited Lecture: Seismic Testing of Structure. Proc.11th European Conference on Earthquake Engineering, Paris, France, (1998), pp. 53-64,

[26] IS 12269: 1987-Indian Standard Specification for 53 Grade Ordinary Portland cement, Bureau of Indian Standards, New Delhi, http://www.iitk.ac.in/ce/test/IS-codes/is.12269.2013.pdf

[27] Granata, P.J., Parvin, A.: An experimental study on Kevlar strengthening of beam-column connections. Journal of Composite Structures 53 (2001) 2, pp.163-171, https://doi.org/10.1016/S0263-8223(00)00187-2

[28] Pampanin, S., Bolognini, D., Pavese, A.: Performance-Based Retrofit Strategy for Existing Reinforced Concrete Frame Systems using Fibre-Reinforced Polymer Composites. Journal of composites for construction, (2007), pp. 1-16.

[29] ACI Committee 318: Building Code Requirements for Structural Concrete (ACI318-M02).American Concrete Institute, 2002.

[30] Park, R.: Ductility of structural concrete. IABSE reports, (1991), pp. 445-456, http://doi.org/10.5169/seals-47669

[31] Hadi, M.N.S., Tran, T.M.: Retrofitting nonseismically detailed exterior beam-column joints using concrete covers together with CFRP jacket. Construction and Building Materials, (2014), pp.161-173.

[32] ACI-ASCE Committee 352 (ACI 352R-02). Recommendations for the design of beam-column connections in monolithic reinforced concrete structures (aci 352r-02). Farmington Hills, Michigan, USA: American Concrete Institute; 2002.

[33] ACI Committee 440: Guide for the design and construction of externally bonded FRP systems for strengthening concrete structures. ACI 440.2R-02. USA: American Concrete Institute, 2012.